AIAA JOURNAL
Vol. 43, No. 5, May 2005

Advanced Test Strategy for Identification and Characterization of Nonlinearities of Aerospace Structures

Dennis Göge* and Ulrich Füllekrug†
Deutsches Zentrum für Luft- und Raumfahrt, D-37073 Göttingen, Germany
Michael Sinapius‡
Deutsches Zentrum für Luft- und Raumfahrt, D-38108 Braunschweig, Germany
Michael Link§
University of Kassel, D-34109 Kassel, Germany
and
Lothar Gaul¶
University of Stuttgart, 70550 Stuttgart, Germany

The development of new, high-performance aerospace structures requires the availability of powerful and efficient methods for dynamic testing. Also, the European aircraft industry is calling for a reduction of the testing times for prototypes without diminishing the accuracy of the test results. As a consequence, substantial improvements in the test strategy of ground vibration and modal survey tests have been developed and applied during the last years. In addition, space agencies like the ESA are interested in advanced measurement techniques, for example, when a spacecraft has to be qualified by a boosted modal survey test. Very high loads are introduced in the structure during these tests, and significant nonlinear behavior of the spacecraft can sometimes be observed. A test strategy is presented that can be used to identify and characterize nonlinear, structural behavior during modal testing. The method assumes a weak non-linear behavior and operates in modal space. The approach can replace the common analysis by linearity plots that are utilized during modal survey testing of aerospace structures. The proposed test strategy supplies much more information on the nonlinear behavior than the common procedure and allows for a reduction in the test duration.

Nomenclature

$[C]$	=	physical linear damping matrix
$[C_{\mathrm{nl}}]$	=	physical nonlinear damping matrix
$[c]$	=	generalized linear damping matrix
c_{eq}	=	equivalent linear viscous damping
c_r	=	generalized viscous damping of mode r
$\{F\}$	=	physical excitation force vector
$\{f\}$	=	generalized excitation force vector
f_r	=	generalized force of mode r
$H(\omega)$	=	frequency response function
i, j	=	integers
$[K]$	=	physical linear stiffness matrix
$[K_{\mathrm{nl}}]$	=	physical nonlinear stiffness matrix
$[k]$	=	generalized linear stiffness matrix
k_{eq}	=	equivalent linear stiffness
k_r	=	generalized stiffness of mode r
$[M]$	=	physical mass matrix
$[m]$	=	generalized mass matrix
m_r	=	generalized mass of mode r
N_c, N_s	=	Fourier coefficients
nr	=	number of modes
$\{q\}$	=	generalized displacement vector
$\{\dot{q}\}$	=	generalized velocity vector
$\{\ddot{q}\}$	=	generalized acceleration vector
$Re(\ )$	=	real part
$\{u\}$	=	physical displacement vector
$\{\dot{u}\}$	=	physical velocity vector
$\{\ddot{u}\}$	=	physical acceleration vector
$\{\delta\}$	=	total nonlinear restoring force vector
δ_c	=	nonlinear damping force
$\{\delta_c\}$	=	nonlinear damping force vector
δ_k	=	nonlinear restoring force
$\{\delta_k\}$	=	nonlinear restoring force vector
ε, γ	=	nonlinear coefficients
ζ_r	=	viscous damping ratio of mode r in %
$[\phi]$	=	modal matrix, contains eigenvectors $\{\phi\}_r$ as columns
$\{\phi\}_r$	=	real normal mode r
ω	=	excitation frequency
ω_r	=	resonance frequency of mode r
$\{\ \}^T$	=	row vector

Subscripts

amp	=	amplitude
c	=	damping
cj	=	Fourier coefficient j (cosine)
cub	=	cubic
eq	=	equivalent
gen	=	generalized
h	=	translational degree of freedom
id	=	identified
in	=	inner part of the restoring force in case of piecewise linear stiffness
lin	=	linear

Received 7 October 2003; revision received 10 August 2004; accepted for publication 15 August 2004.

*Research Scientist, Institut für Aeroelastik, Bunsenstrasse 10; Dennis.Goege@dlr.de.
†Research Scientist, Institut für Aeroelastik, Bunsenstrasse 10; Ulrich.Fuellekrug@dlr.de.
‡Professor, Institut für Strukturmechanik, Lilienthalplatz 7; Michael.Sinapius@dlr.de.
§Professor, Department of Civil Engineering, Lightweight Structures and Structural Mechanics Laboratory, Mönchebergstraße 7; link@uni-kassel.de.
¶Professor, Institute A of Mechanics, Pfaffenwaldring 9; gaul@mecha.uni-stuttgart.de.

max	=	maximum
out	=	outer part of the restoring force in case of piecewise linear stiffness
r	=	actual mode number
sj	=	Fourier coefficient j (sine)
α	=	rotational wing degree of freedom
β	=	rotational control-mount degree of freedom

I. Introduction

VIBRATION tests on aircraft prototypes or spacecraft structures like satellites or launcher components are performed with the purpose of experimentally investigating the structural dynamics behavior and identifying the modal parameters. Linear dynamic behavior of the structure is usually assumed in the applied methods. In practice, most of the investigated and tested structures exhibit some nonlinear behavior. Such nonlinear behavior can occur, for example, as a result of hydraulic systems in control surfaces (aircraft) or free play and different connection categories (e.g., welded, bolted) within joints. A suitable and commonly used procedure to characterize the nonlinear behavior of specific modes in a ground vibration test is to perform normal-mode force appropriation (or so-called phase resonance testing). Here, the structure is harmonically excited by means of an excitation force pattern appropriated to a single mode of vibration. When analyzing the harmonic components of the excitation frequency, the harmonic balance method is technically realized, and a kind of linearization is performed. The nonlinear behavior is then investigated in terms of so-called linearity plots in which the resonance frequency of a mode is plotted as a function of the excitation level. In Ref. 1 it was shown that linearity plots give helpful information about deviations from structural dynamics linearity. Nevertheless, linearity plots do not reveal the source and characteristic of nonlinearities, for example, if damping or stiffness or both kind of nonlinearities are present in the system. Moreover, measuring and creating linearity plots is time consuming. The INTL (identification of nonlinearities by time-series based linearity plots) test strategy is presented in this paper. Within the strategy an identification approach is introduced that is based on the force-state mapping approach.[2] This approach is used to identify modal, nonlinear parameters and characterize the nonlinearity for a single mode of vibration. The advantage of the method is that it can identify any type of nonlinearity, including discontinuous functions, even when stiffness and damping nonlinearities occur together in a single mode. In the second step of the test strategy, linearity plots are created from the restoring force plot by using the harmonic balance method. The INTL strategy and its utilization during modal identification testing are described. The application of the method is illustrated by a simulated aeronautical and a real space structure example. The benefits and the limitations are discussed.

II. Detection and Identification of Nonlinearities

To completely characterize a structure like an aircraft from a structural dynamics point of view, it it neccessary to take four steps: 1) detection, 2) identification, 3) verification, and 4) validation. If we focus on nonlinear structures, the nonlinearities (here: weak nonlinearities) have to be detected in the first step. Nonlinearities can be detected by direct or indirect methods. Direct methods are based on for example, the Hilbert transform[3,4] or an indicator function such as the sig-function.[5] The wavelet transform[6] or the force-state mapping approach[2] are also direct methods that can be used to detect nonlinearities.

The indirect methods use linearity tests and check their violation. They are based on the superposition principle, reciprocity or on the Nyquist plot (see Ref. 7).

Once the nonlinearities are detected, the question remains of how to model them. The identification process is a construction process where a mathematical model is the output. If the mathematical model is known, the identification becomes the parameter estimation. Once again, we distinguish between direct and indirect (model updating) parameter estimation.

Many approaches for the direct identification of nonlinear parameters are proposed. The direct methods aim at fitting the system parameters by using the input (forces) and the output [e.g., frequency response functions (FRFs)] of the system in the time or frequency domain within one step. Some of the main approaches currently in use for nonlinear identification are summarized in this paragraph.

The NARMAX (nonlinear autoregressive moving average with exogenous inputs) models[8] are based on discrete time and are nonlinear versions of the autoregressive moving average (ARMA) models that are used in linear parameter identification. A suitable model to represent physical, lumped parameter, nonlinear systems with few degrees of freedom is based on the force-state mapping approach.[2] In Ref. 2 a nonlinear restoring force is curve fitted using Chebyshev polynomials. This method is also used in Ref. 9 in order to identify the nonlinear stiffness and damping parameters of a joint in physical space. An extension of the force-state mapping approach is the constant-level-identification approach presented in Ref. 10. This parametric approach can be used for the identification of mutiple-degree-of-freedom systems with any type of nonlinearity. A completely different approach is the so-called nonlinear normal modes,[11,12] which represents functions of the momentums. Higher-order frequency response functions[13,14] or the reverse-path (RP) method[15] can be used for the identification of nonlinear systems in the frequency domain. An extension of the RP method for the identification of multi-degree-of-freedom systems is the conditioned reverse-path method presented in Ref. 16. In Ref. 17 a method is proposed that yields a reduced modal model. This model extends the linear modal model with additional polynomial nonlinear stiffness terms. A good overview of direct identification methods is given in Ref. 18, whereas Ref. 19 gives a detailed description and insight into a wide variety of different methods.

The indirect identification methods aim at fitting the parameters of an initial analytical model (e.g., finite element model) in such a way that the test/analysis differences are minimized. This process is iterative and is called model updating. In contrast to the direct identification methods for nonlinear systems, the indirect identification methods for nonlinear systems are still under development and are far from being state of the art. In Refs. 20 and 21 time-domain data are used within the model updating process of nonlinear models. The identification of the modal model of a weak nonlinear structure is presented in Ref. 22. The identification of local stiffness and damping characteristics in large-scale finite element models using FRFs is shown in Refs. 23 and 24. A survey of local nonlinear models describing structural joints has been recently reviewed.[25,26] Once the parameters are identified, the generated model has to be verified. The verification is done by comparing analytical and test data like eigenfrequencies or FRFs.

In the last step the analytical model is validated. The validation process comprises the check of the analytical model with regard to the requirements posed on the model. The validation process strongly depends on the model's final utilization. An analytical model can be considered validated if it is an accurate representation of the real world from the perspective of the intended model application. Typical requirements on validated analytical models are defined in Ref. 27.

In this paper we focus on the detection, identification, and verification. An identification approach for nonlinear modal multi-degree-of-freedom systems is presented. For complex, lightly damped structures with weak nonlinearities, the mode shapes can be classified into different groups as shown in Ref. 17: 1) linear, proportionally damped modes that are well separated in frequency; 2) linear, proportionally damped modes that are very close or identical in frequency; 3) linear, nonproportionally damped modes that are usually fairly close in frequency (significant damping coupling); 4) uncoupled modes that are influenced by nonlinear effects; and 5) coupled modes that are influenced by nonlinear effects.

Most of the modes of a real, complex aerospace structure behave linearly so that identification using the classical, linear methods is possible. Nevertheless, some modes show significant nonlinear behavior, which makes it impossible to adopt linear theory. In this paper we focus on the identification of the uncoupled modes that are

influenced by nonlinear effects. Nevertheless, it is possible to also identify nonlinear, cross-coupling terms with the presented method.

III. Modal Space Identification Approach Within INTL

A. Theoretical Background

In this section the theoretical background of the identification approach is described. The identification approach used within the INTL strategy is based on the force-state mapping approach.[2] When considering a nonlinear, elastomechanical structure discretized with n physical degrees of freedom (DOF), the equation of motion in physical space for this dynamic system including stiffness and damping nonlinearties is

$$[M]\{\ddot{u}(t)\} + [C]\{\dot{u}(t)\} + [C_{\mathrm{nl}}(\{\dot{u}(t)\})]\{\dot{u}(t)\} \cdots + [K]\{u(t)\} + [K_{\mathrm{nl}}(\{u(t)\})]\{u(t)\} = \{F(t)\} \quad (1)$$

where $\{F(t)\}$ is the vector of the excitation forces, $\{u(t)\}$ is the vector of physical displacements, and the dot represents the time derivative. Equation (1) can then be transformed to linear modal space using the modal matrix of the associated linear, undamped system:

$$\{u(t)\} = \sum_{r=1}^{n} \{\phi\}_r q_r(t) = [\phi]\{q(t)\} \quad (2)$$

where $[\phi]$ is the time-independent modal matrix consisting of n modes from the underlying linear system and $\{q(t)\}$ is a time-dependent vector of generalized coordinates that represents the modal amplitudes. Only the modes $nr \ll n$ within the frequency range of interest are important. Inserting the truncated modal expansion into the system equations of motion and premultiplying by the transpose of the modal matrix $[\phi]^T$ yields

$$[\phi]^T[M][\phi]\{\ddot{q}(t)\} + \left([\phi]^T[C][\phi] + [\phi]^T[C_{\mathrm{nl}}][\phi]\right)\{\dot{q}(t)\} \cdots + \left([\phi]^T[K][\phi] + [\phi]^T[K_{\mathrm{nl}}][\phi]\right)\{q(t)\} = [\phi]^T\{F(t)\} \quad (3)$$

With the orthogonality properties of the modes, the equation of motion is transformed in modal space

$$[m]\{\ddot{q}(t)\} + [c]\{\dot{q}(t)\} + [k]\{q(t)\} + \{\delta(t)\} = \{f(t)\} \quad (4)$$

The mass and the stiffness matrix are diagonal, and the generalized damping matrix is also diagonal for the proportionally damped systems. $\{f(t)\}$ is the vector of modal excitation forces, and $\{\delta(t)\}$ is the vector of generalized, nonlinear restoring forces in modal space including stiffness and damping nonlinearities. If there is only a stiffness nonlinearity in the system, the nonlinear restoring force is simply called nonlinear stiffness force ($\{\delta_k(t)\}$). In case of damping nonlinearities only, the nonlinear restoring force is simply called nonlinear damping force ($\{\delta_c(t)\}$). For the sake of simplicity, the off-diagonal terms of $[c]$ are disregarded in a first step, which yields an uncoupled equation of motion for each mode:

$$m_r\ddot{q}_r(t) + c_r\dot{q}_r(t) + k_r q_r(t) + \delta_r(t) = f_r(t), \qquad r = 1, 2, \ldots, nr \quad (5)$$

Normal-mode force appropriation (sine dwell testing) is used during modal survey testing in order to determine the modal parameters of the undamped system.[28] Normal-mode force appropriation is also a common procedure in the aerospace industry in order to investigate the linearity of a specific mode shape (see Ref. 1). The fundamental idea of sine dwell testing is to harmonically excite the structure by an external force vector. The dynamic response is dominated by the fundamental harmonic and has a phase shift with respect to the external force vector. When all dynamic displacement responses have a phase shift of ± 90 deg with respect to the excitation, the phase resonance criterion is fulfilled. This means that the external forces have to be applied to the structure to compensate internal damping. During the tuning process, the phase resonance condition is observed by a weighted average of all measured structural responses given by the mode indicator function (MIF)[29,30]

$$\mathrm{MIF} = 1 - \frac{\{|Re(u_{\mathrm{amp}})|\}^T \cdot \{|u_{\mathrm{amp}}|\}}{\{|u_{\mathrm{amp}}|\}^T \cdot \{|u_{\mathrm{amp}}|\}}, \qquad 0 \le \mathrm{MIF} \le 1 \quad (6)$$

The MIF becomes 1 in the case of a perfectly tuned mode. If a mode behaves nonlinearly (e.g., as a result of freeplay in junctions), which is common during modal survey testing of large aerospace structures, the phase resonance criteria is not fulfilled (MIF < 1). Nevertheless, it is also valid to investigate such a mode within the INTL strategy. The time-domain data of the appropriated mode shapes are used for the identification approach, which is presented next. The fundamental idea of the identification approach is to use the identified generalized mass, damping, and stiffness of an appropriated mode shape and to identify the nonlinear stiffness and/or damping terms of the mode in modal space. If the identification process is performed in two steps, the stiffness and damping nonlinearities can be efficiently identified.

First, Eq. (5) is rewritten in the time domain as

$$\delta_r(t) = -m_r\ddot{q}_r(t) - c_r\dot{q}_r(t) - k_r q_r(t) + f_r(t) \quad (7)$$

where m_r, c_r, and k_r are identified for example from the vector polar plot curve fit, evaluation of real part slopes, or from the complex power method (see Refs. 31 and 32). The $\ddot{q}_r(t)$ is calculated from the physical acceleration responses $\{\ddot{u}(t)\}$ and the eigenvector $\{\phi\}_r$ by Eq. (2). The generalized velocity $\dot{q}_r(t)$ and the generalized displacement $q_r(t)$ response of the mode shape can be obtained by integration of the filtered, generalized acceleration responses. In this paper a high-pass Butterworth filter was used (see Ref. 33). The modal excitation force is calculated from measured eigenvectors and excitation forces. The identification method is carried out in two steps because stiffness and damping nonlinearities can be present simultaneously in the mode shape. In the first step the nonlinear stiffness is identified if it is present in the mode shape. For this purpose the nonlinear restoring force $\delta_r(t)$ is plotted vs the generalized displacement $q_r(t)$. If a polynominal stiffness (e.g., cubic stiffness) nonlinearity is present, the nonlinearity type is visible in the force-displacement plot. In the case where a piecewise linear stiffness characterization is more appropriate, the linear stiffness term is best merged into the nonlinear restoring force:

$$\delta_r(t) = -m_r\ddot{q}_r(t) - c_r\dot{q}_r(t) + f_r(t) \quad (8)$$

For practical applications it is beneficial to plot both restoring functions of Eqs. (7) and (8). This helps avoid interpretation errors during the curve-fitting procedure. An approximation of the actual nonlinearity is required for the identification, which can realized by a least-squares curve fit. If, for example, a polynominal stiffness (cubic stiffness) best fits the stiffness nonlinearity, the identification equation is

$$\begin{Bmatrix} \delta_{k,r,1} \\ \delta_{k,r,2} \\ \vdots \\ \delta_{k,r,m} \end{Bmatrix} = \begin{Bmatrix} q_{r,1}^3 \\ q_{r,2}^3 \\ \vdots \\ q_{r,m}^3 \end{Bmatrix} k_{\mathrm{nl},r} \quad (9)$$

where m is the number of time steps. In the case where neither a stiffness nor a damping nonlinearity is present in the mode shape, the plot might show only numerical noise because the restoring force should theoretically be equal to zero. Whenever the damping is nonlinear, the previously identified nonlinear stiffness is written on the right-hand side of Eq. (7), which results in

$$\delta_r(t) = \delta_{c,r}(t) = -m_r\ddot{q}_r(t) - c_r\dot{q}_r(t) - k_r q_r(t) - k_{\mathrm{nl},r}q_r^3(t) + f_r(t) \quad (10)$$

Then, the nonlinear restoring force $\delta_r(t)$, which is now simply the damping force $\delta_{c,r}(t)$, is plotted vs the generalized velocity $\dot{q}_r(t)$. Whenever a damping nonlinearity is present in the mode, the type of

nonlinearity is visible in the force-velocity plot. Again, the nonlinear term can be identified by a least-squares curve fit. If, for example, a polynominal damping (quadratic damping) best characterizes the damping nonlinearity, the identification equation is

$$\begin{Bmatrix} \delta_{c,r,1} \\ \delta_{c,r,2} \\ \vdots \\ \delta_{c,r,m} \end{Bmatrix} = \begin{Bmatrix} \dot{q}_{r,1}|\dot{q}_{r,1}| \\ \dot{q}_{r,2}|\dot{q}_{r,2}| \\ \vdots \\ \dot{q}_{r,m}|\dot{q}_{r,m}| \end{Bmatrix} c_{\mathrm{nl}} \tag{11}$$

Again, the plot might only show numerical noise when neither a stiffness nor a damping nonlinearity is present in the mode shape because the nonlinear damping force should theoretically be equal to zero. It is reasonable to identify the nonlinear parameters by this two-step approach because the nonlinear stiffness forces are much higher than the nonlinear damping forces in most practical applications. It is obvious that the damping forces play only a secondary role in the force-displacement plot. Vice versa, the nonlinear stiffness forces dominate the force-velocity plot. This is the reason why the nonlinear stiffness parameters have to be identified in the first step.

To obtain the modal model for the identification process, the physical equation of motion was premultiplied by the modal matrix $[\phi]^T$ or the respective mode $\{\phi\}_r^T$. However, the question remains of which mode shape has to be used for the investigated mode. Is the appropriated mode from a high or low load level best applicable? A pragmatic answer can be given by Fig. 1, which shows the modes of a civil, two-engine aircraft that behaves nonlinearly.

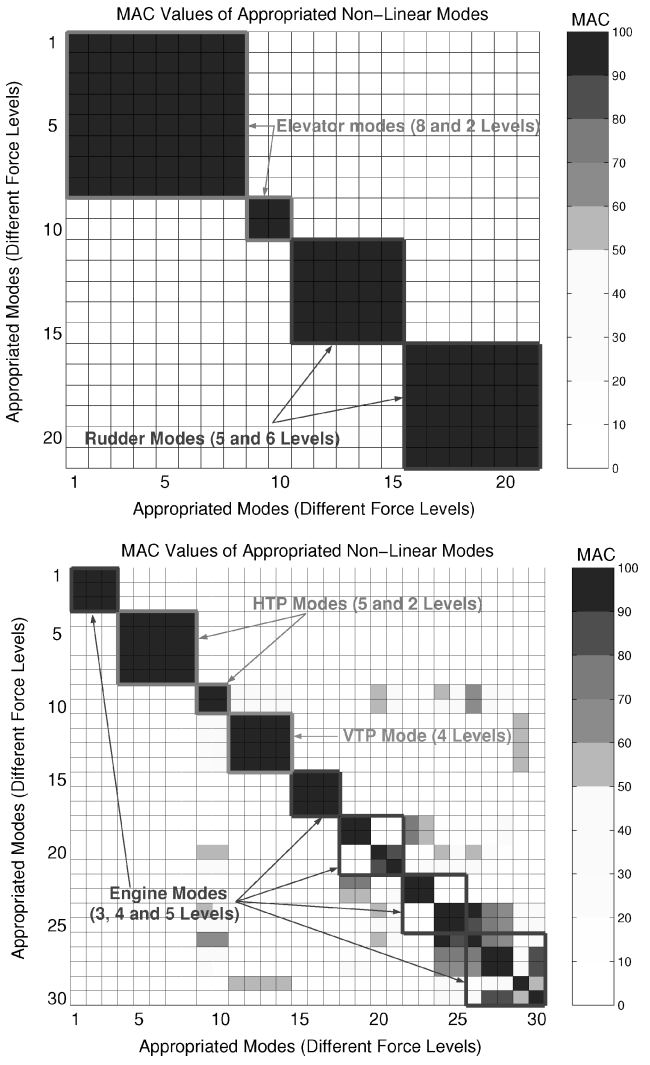

Fig. 1 MAC values of appropriated modes of a civil two-engine aircraft showing nonlinear behavior.

It can be observed that nearly all modes have a modal assurance criterion (MAC) value that is ≈100% for different force levels, with the exception of some of the engine modes. The MAC represents a criterion for the comparison of vector pairs. MAC = 100% denotes that the vectors are equal. That means that the shapes of most modes are unaffected by different force levels, which leads to the conclusion that the mode shape appropriated on the high load level is also valid for the low level. Based on this experience, the INTL approach presupposes that each tuned eigenvector can be used for the underlying linear system. This is important for the last step in the INTL strategy, where a prediction for the low-level appropriated modes is made by using the eigenvector of the mode appropriated on a high-force level.

B. Illustrative Example

A single-degree-of-freedom (SDOF) system is used in this subsection in order to prove that the approach just presented is suitable for identifying nonlinear parameters. It is also used to elucidate the approach. The generalized parameters of the linear system are assumed to be $m_r = 1.5$ kg for modal mass, $k_r = 6.0 \times 10^3$ N/m for modal stiffness, and $c_r = 0.8$ Ns/m for viscous damping. The system includes cubic stiffness nonlinearity and also quadratic damping. The following generalized, nonlinear parameters were chosen: $k_{\mathrm{nl},r} = 10.0 \times 10^7$ N/m^3 and $c_{\mathrm{nl},r} = 14.0$ Ns^2/m^2. Figure 2 shows the appropriated modal acceleration response of the system. The excitation frequency is nearly that of the resonance frequency of the system (MIF ≈ 1). In this simulated test case the velocity and displacement responses are calculated analytically. In the first step, the nonlinear restoring force $\delta_r(t)$ is calculated for each time step using Eqs. (7) and (8). Then, $\delta_r(t)$ is plotted against the displacement response. Figures 3 and 4 show the nonlinear restoring force with and without the linear stiffness term for the nonlinear SDOF system. The cubic characteristic can be clearly seen in both plots. The hysteresis effect is caused by the damping. Whenever neither stiffness nor damping nonlinearity is present in the system, the mode is linear, and the nonlinear restoring force is zero or consists of numerical noise. Next, the nonlinear stiffness term is curve fitted using Eq. (9). Figure 5 shows the curve-fitted restoring force, which corresponds to the nonlinear stiffness force $\delta_{k,r}(t)$. The nonlinear stiffness parameter is identified as the exact value of $k_{\mathrm{nl,id}} = 10.0 \times 10^7$ N/m^3. Next, the restoring force calculated with Eq. (7) is plotted vs the velocity in Fig. 6.

It is not possible to characterize the damping nonlinearity from the shape of the restoring force because it still contains the stiffness nonlinearity. Thus, the nonlinear damping force is calculated using Eq. (10) and plotted against the velocity response (see Fig. 7), which reveals a polynominal characteristic. Finally, the nonlinear damping term is curve fitted using Eq. (11). Just as for the nonlinear stiffness, the nonlinear damping parameter is exactly identified with $c_{\mathrm{nl,id}} = 14.0$ Ns^2/m^2. Figure 8 shows the curve-fitted, nonlinear

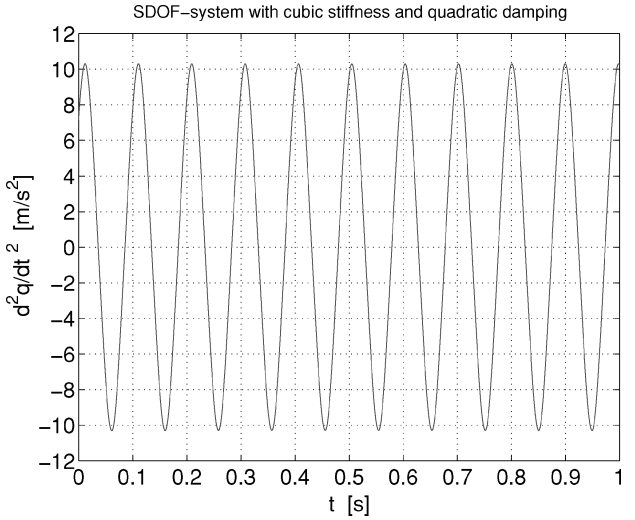

Fig. 2 Modal acceleration response of the nonlinear SDOF system.

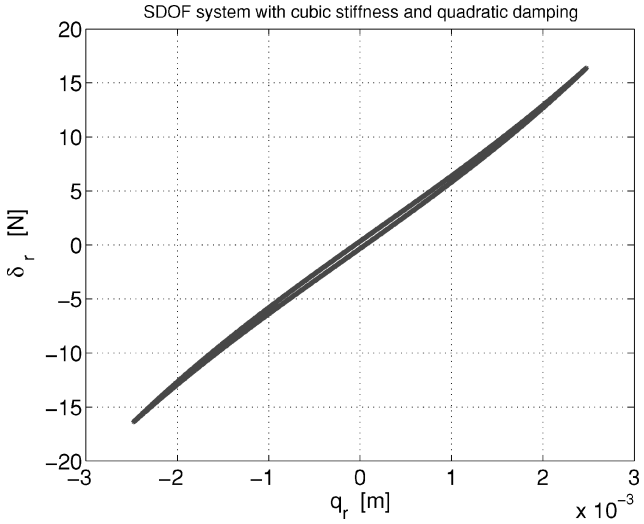

Fig. 3 Simulated nonlinear restoring force including linear stiffness of the nonlinear SDOF system according to Eq. (8).

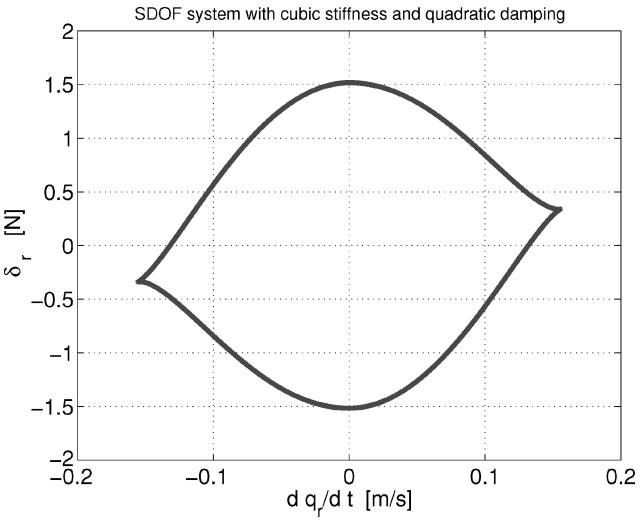

Fig. 6 Simulated nonlinear damping force including nonlinear stiffness of the nonlinear SDOF system according to Eq. (7).

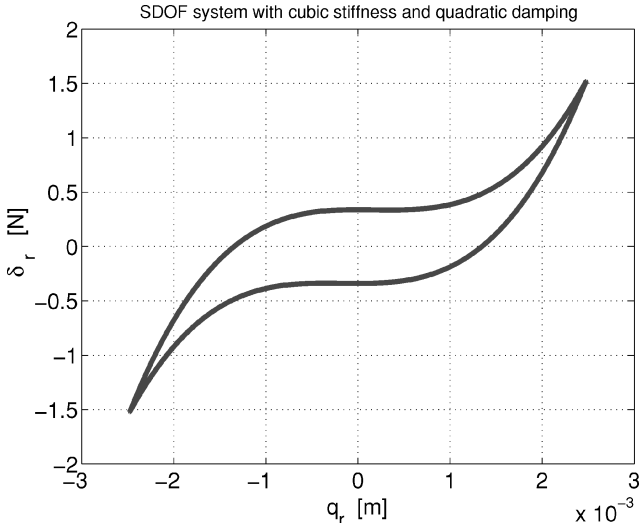

Fig. 4 Simulated nonlinear stiffness force without linear stiffness of the nonlinear SDOF system according to Eq. (7).

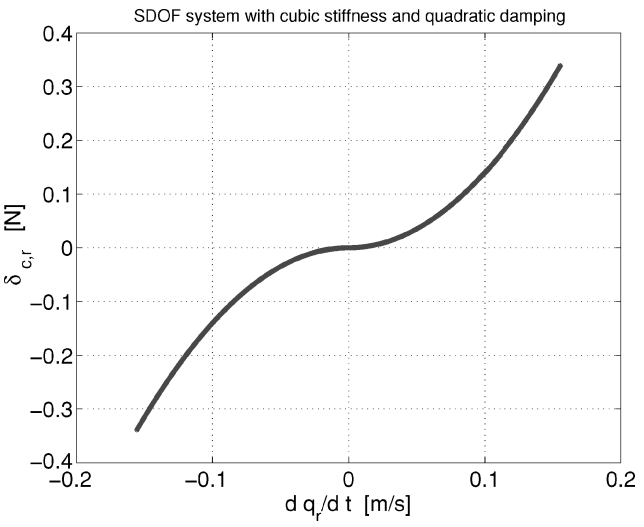

Fig. 7 Simulated nonlinear damping force without nonlinear stiffness of the nonlinear SDOF system according to Eq. (10).

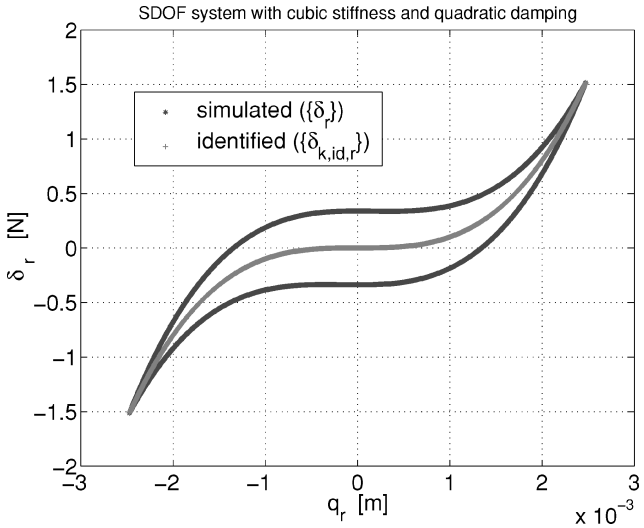

Fig. 5 Simulated and identified nonlinear stiffness force of the nonlinear SDOF system.

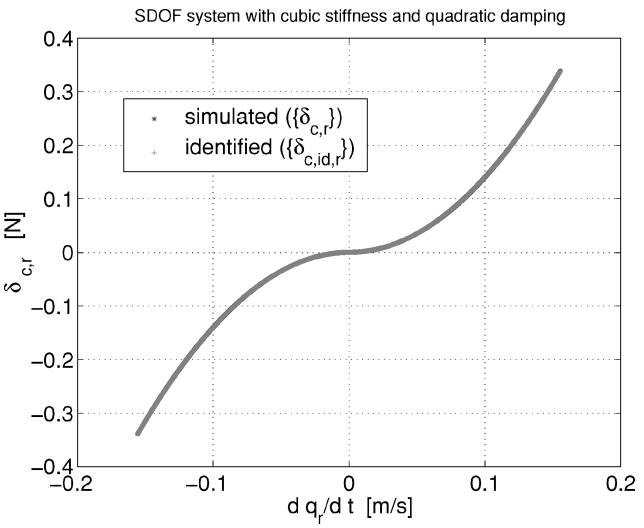

Fig. 8 Simulated and identified nonlinear damping force of the nonlinear SDOF system.

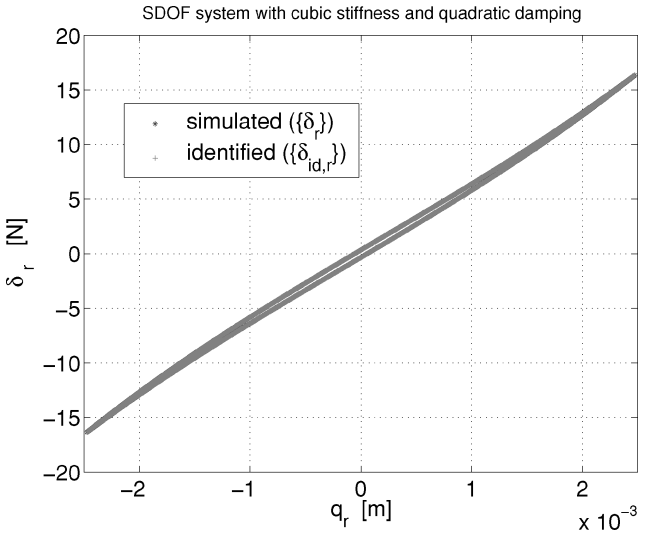

Fig. 9 Simulated and identified restoring force of the nonlinear SDOF system.

damping force, which corresponds to $\delta_{c,r}(t)$. The total simulated and identified restoring force is plotted in Fig. 9 vs the displacement. No deviations between simulated and identified restoring forces can be seen in Figs. 8 and 9 because the simulated and the identified parameters are exactly the same.

The presented approach is not only robust when using noise-free, experimental data. In Ref. 34 it is shown that the restoring force surface method can deal with experimental data from nonlinear systems that have a relatively high signal-to-noise ratio.

IV. Linearity Investigations

In this section the linearity investigations currently used in practice are described first. Then, an alternate kind of linearity plot based on the INTL strategy is presented, and its theoretical background is described.

A. Current Linearity Investigations

Investigation of the structural responses to harmonic excitation is common in the ground vibration tests of large aerospace structures. Harmonic distortion of the responses indicates the presence of nonlinearities. The investigation of the nonlinearities during modal identification nowadays is based on the harmonic balance method. The harmonic balance method[35] is technically realized by harmonic analysis of the responses. Excitation forces are appropriated to the normal mode, and the structure is excited on different force levels. The mode appropriation on different load level delivers resonance frequencies that depend on the load level. Plotting the measured resonance frequencies vs the maximum displacement shows the dependency of the resonance frequency on the load level.

1. *Theoretical Background*

Weak nonlinearities can be described by adding a nonlinear stiffness function $\delta_k(q)$ and a nonlinear damping function $\delta_c(\dot{q})$ to the linear equations of motion

$$m_r\ddot{q}_r + c_r\dot{q} + \delta_c(\dot{q}) + k_r q + \delta_k(q) = f_r(t) \tag{12}$$

The harmonic balance assumes that most of the response energy of a harmonically excited structure is concentrated in the frequency of excitation. Thus the displacement response of the structure can be approximated by

$$q(t) = q_c\cos(\omega t) + q_s\sin(\omega t) \tag{13}$$

The harmonic balance linearizes the nonlinear equations of motion by using an equivalent linear stiffness k_{eq} and an equivalent linear viscous damping c_{eq}

$$k_{\text{eq}}(\hat{q})\,q(t) \approx k_r q + \delta_k(q) \tag{14}$$

$$c_{\text{eq}}(\hat{\dot{q}})\,\dot{q}(t) \approx c_r\dot{q} + \delta_c(\dot{q}) \tag{15}$$

The tuning of mode r is realized by appropriating the excitation force pattern and the excitation frequency ω. If the mode indicator function reaches a sufficient value, the resonance frequency ω_r of the actual load level can be measured. Also, it is possible to measure the generalized parameters m_r and ζ_r.

The amplitude-dependent parameters are usually presented in linearity plots where the vibration amplitude $\hat{q} = \sqrt{(q_c^2 + q_s^2)}$ is plotted as a function of the excitation force represented by the generalized force:

$$f_r = \{\phi\}_r\{F\} \tag{16}$$

To do this, an appropriate and consistent scaling of the eigenvector $\{\phi\}_r$ is required. Relating the vibration amplitude to the generalized force enables modal data from different excitation force patterns to be compared and combined in linearity plots.

In a second diagram the resonance frequency ω_r is depicted as a function of the vibration amplitude $\hat{q}$. The amplitude vs force plot is referred to as amplitude linearity in this paper, whereas the frequency vs amplitude plot is referred to as frequency linearity. The method is applicable as long as a force appropriation to a single mode of vibration is possible. This can be assumed for weak nonlinearities in most cases.

2. *Example*

Figure 10 shows a linearity plot for the horizontal tailplane (HTP) yaw mode of a civil, two-engine aircraft, appropriated on seven different force levels. The upper part of the plot shows the frequency linearity, and the lower part of the plot shows the amplitude linearity. For linear systems the resonance frequency f remains constant with increasing amplitudes u_{amp}, and, simultaneously, the amplitudes rise linearly with the generalized force levels p_{amp}. In Fig. 10 the frequencies, amplitudes, and forces of the different levels are related to the maximum load (index max). The deviation of the HTP yaw mode from linearity can be clearly observed in Fig. 10. The resonance frequency varies with the load level by nearly 4%. The

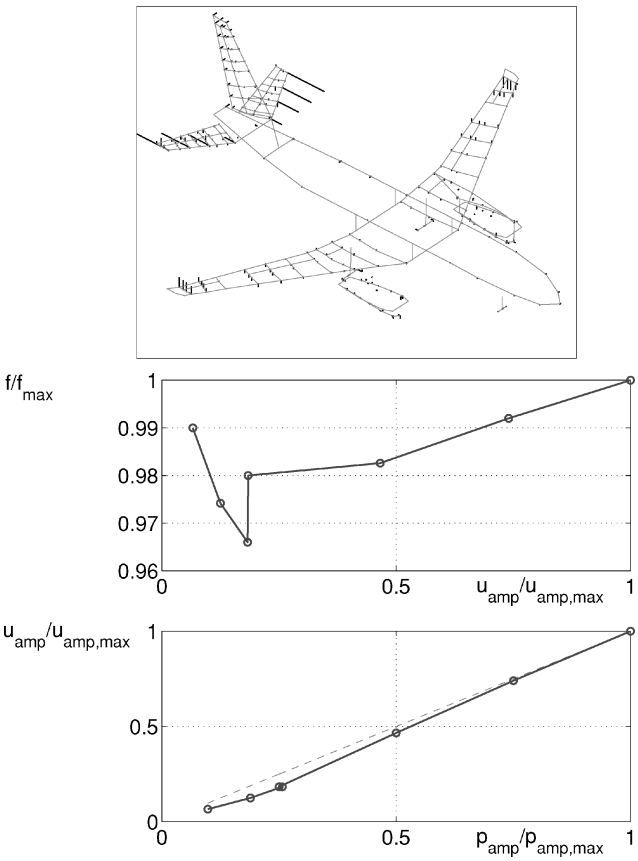

Fig. 10 Linearity plot for the HTP yaw mode of a civil two-engine aircraft.

experimental linearity plots give helpful information about deviations from linearity. Nevertheless, the type of nonlinearity cannot be identified by the linearity plots.[1] Another disadvantage of the current linearity plots is the way of generating them. The mode needs to be appropriated for each force level, which is time consuming, especially if modes are close in frequency. To save testing time, a method for deriving linearity plots from swept-sine testing was recently proposed.[36,37]

B. Alternate Kind of Linearity Investigation

A method is presented in this section, which allows for the analytical calculation of the linearity plots from a mode appropriated at a high force level. Use is made of the identified restoring and damping forces.

1. *Theoretical Background*

Once the curve fitting of the nonlinear restoring forces is successfully completed, an analytical expression for the total restoring function $\delta(q,\dot{q})$ can be established. The analytical expression is composed by linear terms for displacement and velocity as well as by nonlinear terms like quadratic and cubic polynomials. Other functions might be appropriate in special cases. The total restoring function $\delta(q,\dot{q})$ can be written as

$$\delta(q,\dot{q}) = \varepsilon_1 q + \varepsilon_3 q^3 + \cdots + \gamma_1 \dot{q} + \gamma_2 \dot{q}|\dot{q}| + \gamma_3 \dot{q}^3 + \cdots \quad (17)$$

According to the linearization with the harmonic balance method, the displacements and velocities of the rth generalized degree of freedom $q_r(t)$ are assumed to be harmonic [see Eq. (13)]:

$$q(t) = q_c \cos(\omega t) + q_s \sin(\omega t) \quad (18)$$

$$\dot{q}(t) = -q_c \omega \sin(\omega t) + q_s \omega \cos(\omega t) \quad (19)$$

Inserting Eqs. (18) and (19) into Eq. (17) delivers an expression for the total restoring function $\delta(q,\dot{q})$, which is periodic in time. The duration of one period is

$$T = 2\pi/\omega \quad (20)$$

Thus, the total restoring function $\delta(q,\dot{q})$ can be approximated by a Fourier series

$$\delta(q,\dot{q}) = \frac{\delta_{co}}{2} + \sum_{j=1}^{\infty} \delta_{cj} \cos(j\omega t) + \sum_{j=1}^{\infty} \delta_{sj} \sin(j\omega t) \quad (21)$$

The Fourier coefficients can be calculated from

$$\delta_{cj} = \frac{2}{T} \int_0^T \delta(q,\dot{q},) \cos(j\omega t)\, \mathrm{d}t \quad (22)$$

$$\delta_{sj} = \frac{2}{T} \int_0^T \delta(q,\dot{q}) \sin(j\omega t)\, \mathrm{d}t \quad (23)$$

Substituion of the time variable t by $\alpha := \omega t$ leads to

$$\delta_{cj} = \frac{1}{\pi} \int_0^{2\pi} \delta[q(\alpha),\dot{q}(\alpha)] \cos(j\alpha)\, \mathrm{d}\alpha \quad (24)$$

$$\delta_{sj} = \frac{1}{\pi} \int_0^{2\pi} \delta[q(\alpha),\dot{q}(\alpha)] \sin(j\alpha)\, \mathrm{d}\alpha \quad (25)$$

These integrals can be easily computed. The equivalent stiffness and damping values finally follow from

$$k_{eq} = \frac{\delta_{c1} q_c + \delta_{s1} q_s}{q_c^2 + q_s^2} \quad (26)$$

$$c_{eq} = \frac{\delta_{c1} q_s - \delta_{s1} q_c}{\omega\left(q_c^2 + q_s^2\right)} \quad (27)$$

The variation of the displacement amplitude $\hat{q} = \sqrt{(q_c^2 + q_s^2)}$ from 0 to $\hat{q}_{max}$ enables the computation of equivalent stiffness k_{eq} and damping values c_{eq} for each response amplitude.

With the equations

$$\omega_r = \sqrt{k_{eq}/m_r} \quad (28)$$

$$\zeta_r = c_{eq} \Big/ 2\sqrt{k_{eq} m_r} \quad (29)$$

the dependency of resonance frequency ω_r and the viscous damping ratio ζ_r on the response amplitude $\hat{q}$ can be computed. A graphical depiction of functions $\omega_r(\hat{q})$ and $\zeta_r(\hat{q})$ or $\zeta_r(\omega_r)$ offers a good insight into the behavior of the investigated eigenmode.

2. *Features of the Alternate Method*

The described method is capable of characterizing the nonlinearity from the measurement at one single excitation level (the highest excitation force level possible). As a matter of course, no prediction for higher excitation levels is possible, but all force levels that are lower than the measured force level can be investigated. This feature of the method helps reduce the testing time because the time-consuming tuning process for other excitation levels can be avoided. With the purpose of uniquely describing the nonlinear behavior, it is reasonable to depict the resonance frequency vs the displacement amplitude and the viscous damping ratio vs the resonance frequency. The method can be included in the INTL strategy as the last step (Fig. 11). The measurement at a high-excitation force

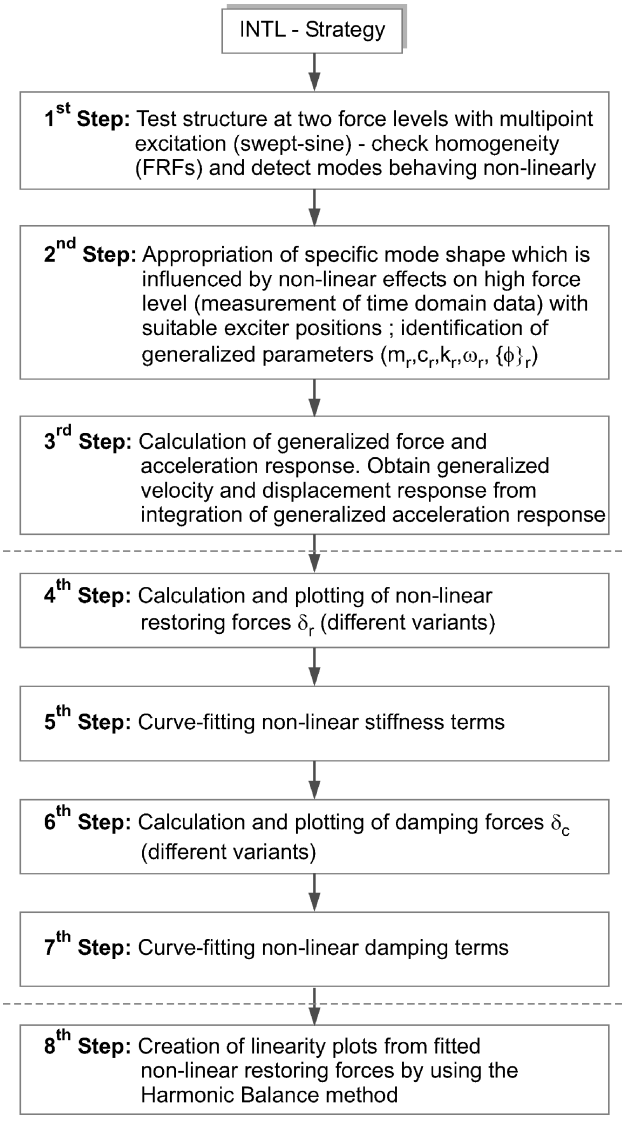

Fig. 11 Flow diagram of advanced test concept INTL.

level during modal identification is quite important because a higher vibration level such as those that occur during flight maneuvers can be reached. From this point of view, the method can also be considered as a validation tool because the complete operation range is covered.

C. Remarks to Mode Coupling

As already mentioned, mode coupling can occur because of a high modal density and structural or damping nonlinearities. This means that the investigated mode shape might not be perfectly appropriated. In Ref. 38 an approach that extends the classical linear force appropriation approach to nonlinear systems is introduced. The excitation in this approach aims to prevent any response other than that in the underlying linear mode shape of interest. The major drawback of this method is that it is rather slow, which makes it inappropriate for modal survey testing of large-scale structures. Nevertheless, classical force appropriation is suitable to identify a complete modal model including weak, nonlinear phenomena. For the identification, the presented approach can be extended in order to deal with cross-coupling terms, which is not straightforward.

V. Applications

Two examples are presented to show the efficiency of the advanced test strategy summarized in Fig. 11. After a simulated example, the approach is applied to a real spacecraft structure.

A. Aeronautical Wing/Control-Surface System

The complete INTL test strategy is applied on a wing/control-surface system, which is well known in aeroelasticity.[39] Figure 12 shows a sketch of the system that has three DOFs. The system has a flexural stiffness k_h for the wing bending and a rotational stiffness k_α for the wing torsion. A control surface is considered as well mounted with a softening piecewise linear stiffness k_β to the wing. The stiffness matrix is written in the following form:

$$[K] = \begin{bmatrix} k_h & 0 & 0 \\ 0 & k_\alpha & 0 \\ 0 & 0 & k_\beta \end{bmatrix} \tag{30}$$

If the rotation at the control mounting is between -1.5×10^{-4} rad $\leq \beta \leq 1.5 \times 10^{-4}$ rad, the stiffness matrix

$$[K] = \begin{bmatrix} 6000 & 0 & 0 \\ 0 & 16{,}000 & 0 \\ 0 & 0 & 4082 \end{bmatrix} \tag{31}$$

is used. This is the stiffness matrix of the so-called associated linear system. If the rotation at the control mounting is $\beta > 1.5 \times 10^{-4}$ rad or $\beta < -1.5 \times 10^{-4}$ rad, then the stiffness matrix accounting for k_β stiffness reduction reads as

$$[K] = \begin{bmatrix} 6000 & 0 & 0 \\ 0 & 16{,}000 & 0 \\ 0 & 0 & 2082 \end{bmatrix} \tag{32}$$

Thus, the system is characterized by a piecewise linear control mounting stiffness k_β. The mass matrix is fully populated:

$$[M] = \begin{bmatrix} 12.0000 & 1.2000 & 0.0600 \\ 1.2000 & 3.0000 & 0.2868 \\ 0.0600 & 0.2868 & 0.2448 \end{bmatrix} \tag{33}$$

Proportional viscous damping with

$$[C] = [K] \times \frac{1}{1000} = \begin{bmatrix} 6.000 & 0 & 0 \\ 0 & 16.000 & 0 \\ 0 & 0 & 4.082 \end{bmatrix} \tag{34}$$

is assumed. After solving the eigenvalue problem for the associated linear system, the modal matrix and the eigenfrequencies of the system are obtained:

$$[\phi_{\text{lin}}] = \begin{bmatrix} -1.0000 & -0.1134 & 0.0088 \\ -0.0413 & 1.0000 & -0.1357 \\ -0.0090 & 0.5334 & 1.0000 \end{bmatrix} \tag{35}$$

$$f_1 = 3.5514 \text{ Hz}, \qquad f_2 = 11.5903 \text{ Hz}, \qquad f_3 = 22.3819 \text{ Hz} \tag{36}$$

The three modes are the wing bending ($f_1 = 3.5514$ Hz), wing torsion ($f_2 = 11.5903$ Hz), and the rudder rotation ($f_3 = 22.3819$ Hz). Now the generalized matrices can be calculated. The generalized stiffness matrices are

$$[k] = \begin{bmatrix} 6028 & 0 & 0 \\ 0 & 17{,}239 & 0 \\ 0 & 0 & 4377 \end{bmatrix} \tag{37}$$

$$[k] = \begin{bmatrix} 6027 & 10.000 & 18.0 \\ 10.0 & 16670 & -1067 \\ 18.0 & -1067 & 2377 \end{bmatrix} \tag{38}$$

The generalized stiffness matrix for the condition $\beta > 1.5 \times 10^{-4}$ or $\beta < -1.5 \times 10^{-4}$ [Eq. (38)] now shows some small coupling terms.

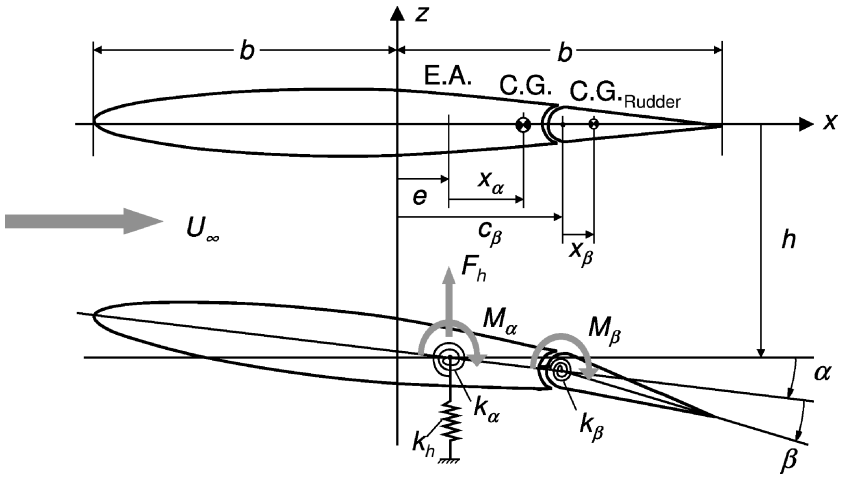

Fig. 12 Aeroelastic wing/control-surface system.

These occur as a result of the multiplication of the physical stiffness matrix of Eq. (32) with the modal matrix [Eq. (35)] of the underlying linear system. Equation (35) was generated with the stiffness matrix according to Eq. (31). The generalized mass and damping matrices are

$$[m] = \begin{bmatrix} 12.1055 & 0 & 0 \\ 0 & 3.2505 & 0 \\ 0 & 0 & 0.2213 \end{bmatrix} \tag{39}$$

$$[c] = \begin{bmatrix} 6.0276 & 0 & 0 \\ 0 & 17.2386 & 0 \\ 0 & 0 & 4.3772 \end{bmatrix} \tag{40}$$

The eight steps of the INTL strategy (Fig. 11) are necessary in order to obtain the frequency and damping linearity plot of the mode, which behaves nonlinearly.

First Step

The system is excited at the control surface using swept-sine excitation with two different force levels. The sum-FRFs

$$\text{Sum-FRF} = \sum_i H_i(\omega) \tag{41}$$

of both levels are calculated and plotted in order to check homogeneity (see Fig. 13). Only two modes respond as a result of the excitation on the rudder (wing torsion and rudder rotation). The FRFs are distorted in the region of the rudder mode (mode no. 3). This mode exhibits nonlinear behavior. Thus, only the third mode has to be considered in the following steps.

Second Step

The rudder rotation mode is appropriated with an excitation force that is 3.3 times higher than the highest excitation force of the swept-sine run. The excitation frequency is equal to the resonance frequency of the rudder rotation mode $f_3 = 17.90$ Hz. The MIF has the value 0.993. The mode shape and a few seconds of the acceleration responses are stored for the subsequent analysis like under real testing conditions. Simultaneously, the generalized mass, damping, and stiffness are identified. The generalized stiffness is calculated by the resonance frequency and the generalized mass:

$$k_{\beta,3} = \omega_3^2 \times m_3 = 2799.7 \text{ N/m} \tag{42}$$

Third Step

The generalized force and generalized acceleration are obtained by premultiplying the physical force vector and acceleration responses with the measured eigenvector $\{\phi\}_3$. After that, the generalized velocity and displacement response in the time domain are calculated by integrating the generalized acceleration response.

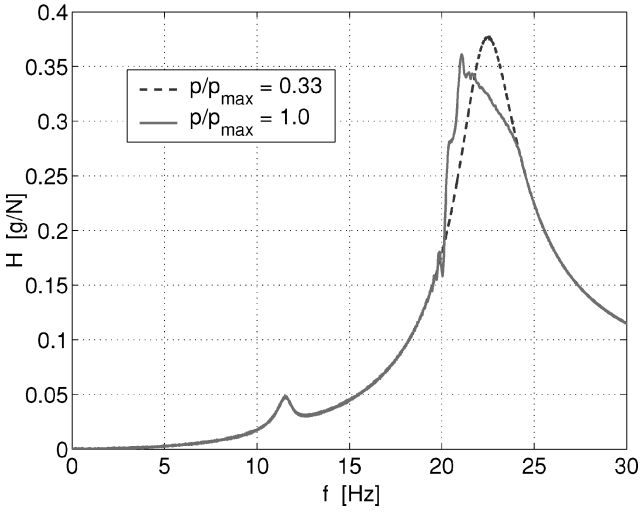

Fig. 13 Sum FRFs of the wing/control-surface system.

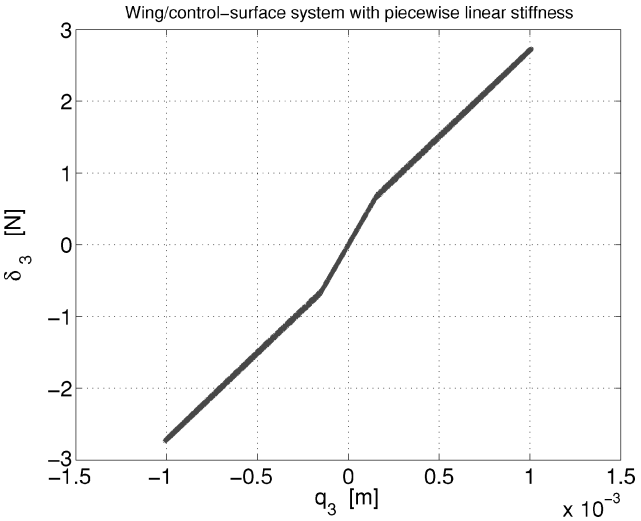

Fig. 14 Simulated nonlinear restoring force including linear stiffness of the wing/control-surface system.

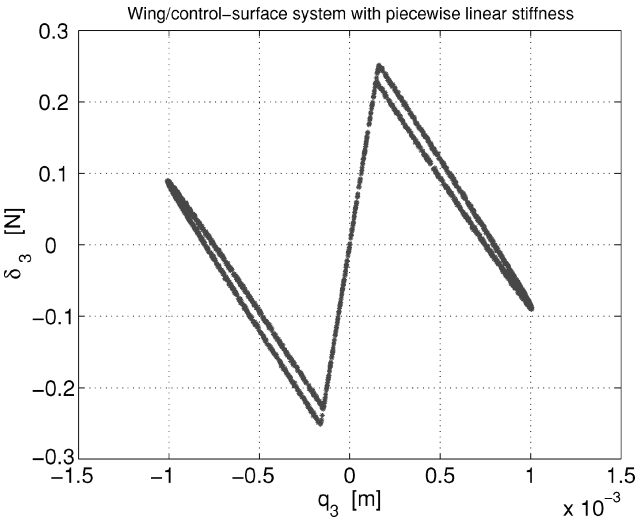

Fig. 15 Simulated nonlinear stiffness force without linear stiffness of the wing/control-surface system.

Fourth Step

The identification process starts with the calculation of the nonlinear restoring forces $\delta_3(t)$ for each time step [Eqs. (7) and (8)]. These forces are plotted vs the generalized displacements (see Figs. 14 and 15). The just mentioned difficulties for systems with piecewise linear stiffnesses can be clearly seen in Fig. 15. When the linear stiffness term is not included in the nonlinear restoring force, the output cannot be interpreted. Figure 14 shows the nonlinear restoring force including the linear stiffness term. The introduced nonlinearity can be clearly seen and interpreted as a piecewise linear stiffness.

Fifth Step

The nonlinear restoring force shown in Fig. 14 is now used to curve fit the nonlinear stiffness terms of the mode shape. The stiffness term of the inner part of the restoring force is exactly identified with $k_{\text{in,id}} = 4377$ N/m. The stiffness term of the outer part of the restoring force is identified with $k_{\text{out,id}} = 2424$ N/m, which represents the entire system because the system was transformed with the mode shape of the underlying linear system (stiffness k_{in}). Figure 16 shows the simulated nonlinear restoring force $\delta_3(t)$ and

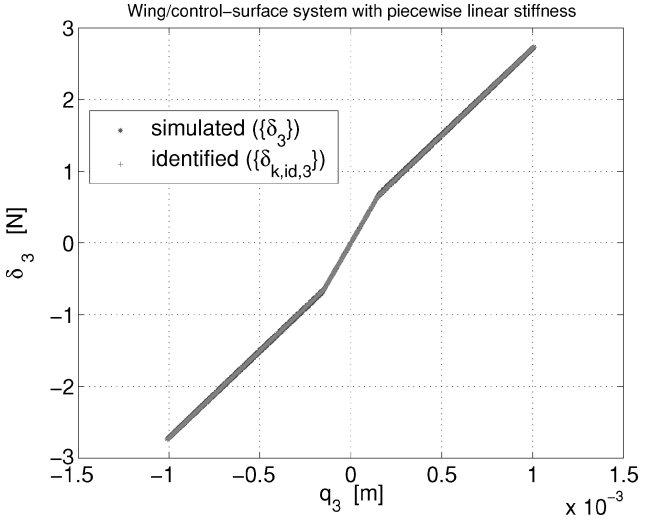

Fig. 16 Simulated nonlinear stiffness force and identified nonlinear stiffness force of the wing/control-surface system.

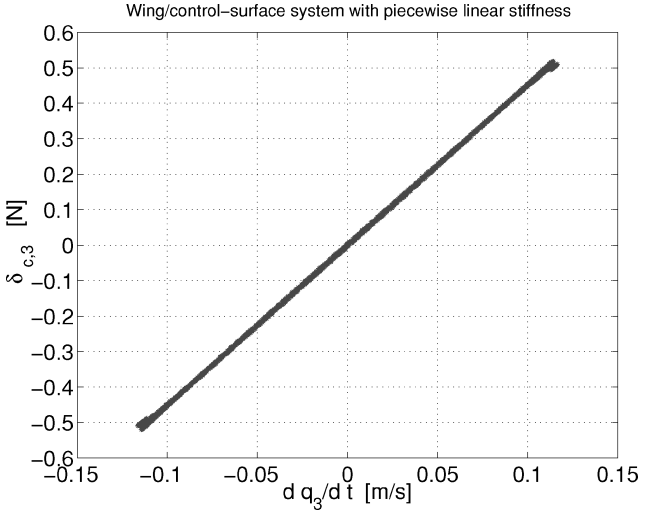

Fig. 17 Simulated nonlinear damping force without identified nonlinear stiffness force of the wing/control-surface system.

the identified nonlinear stiffness force $\delta_{k,\mathrm{id},3}(t)$ of the appropriated mode shape, which shows exact agreement because the parameter was precisely identified.

Sixth Step

The nonlinear damping force of the mode is calculated next without consideration of the identified stiffness terms. Fig. 17 shows the simulated damping force plotted vs the generalized velocity. The damping force is linear, but for the high velocities something like numerical noise can be observed. This is because of the small coupling between the rudder rotation mode and the wing torsion mode that occurs for high velocities. The reason for the coupling terms is that the system is no longer proportionally damped because of the changing stiffness. Nevertheless, the coupling is negligible.

Seventh Step

Figure 18 depicts the curve-fitted, nonlinear damping force $\delta_{c,\mathrm{id},3}(t)$ in comparison to the simulated, nonlinear damping force $\delta_{c,3}(t)$. The identified modal damping term is $c_{\mathrm{id}} = 4.4831$ Ns/m, which deviates about 2% from the underlying linear system. This deviation is caused by mode coupling.

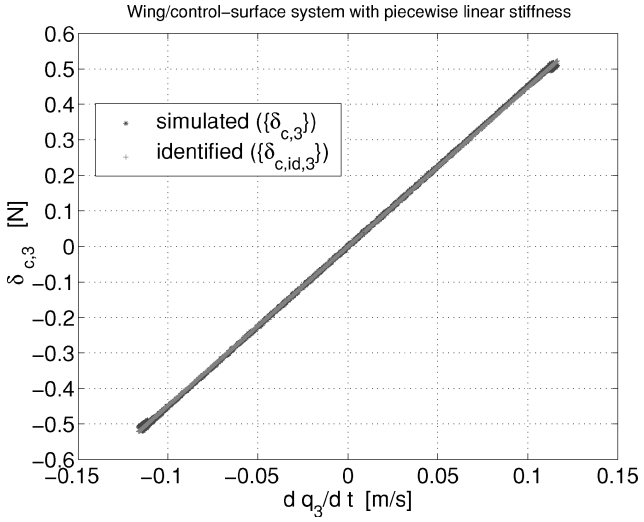

Fig. 18 Simulated and identified nonlinear damping force of the wing/control-surface system.

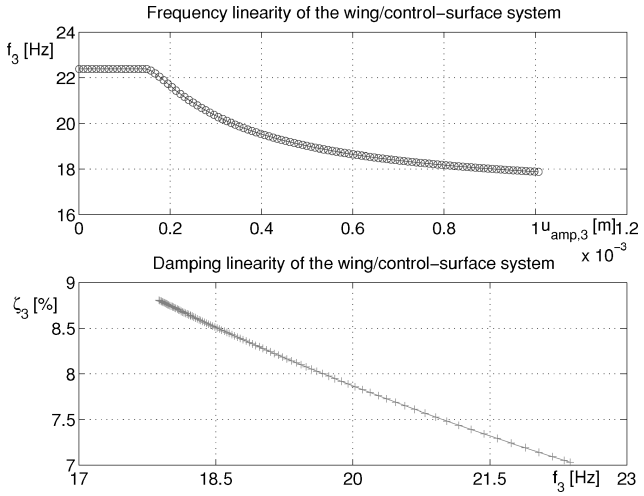

Fig. 19 Linearity plots of the wing/control-surface system.

Eighth Step

The dependency of the frequency and damping on the excitation level is computed as just explained. One-hundred-ten points between zero and the maximum amplitude were utilized for the generation of the plots. The linearity plots are shown in Fig. 19. For small displacement amplitudes the system is linear, and the resonance frequency remains constant. Above the level of 1.5×10^{-4}, the resonance frequency decreases because of the reduction of the stiffness. The change of the resonance frequency has a maximum at the beginning of the reduced stiffness. For even higher displacements the resonance frequency approaches a constant level. The damping linearity plot shows that the damping decreases for decreasing resonance frequencies.

B. Spacecraft Structure European Robotic Arm

Experimental data from the European Robotic Arm (ERA), which is part of the International Space Station, are used to underline the efficiency of the presented INTL strategy. ERA is an approximately 12-m-long, relocatable robot arm with a mass of 630 kg. It is used for the inspection, handling, and installation of in-orbit replaceable units. A boosted modal survey test was performed in order to qualify the interface between ERA and launcher.[40] During launch, ERA is attached to the pressurized module of the Science Power Platform by means of six launcher fixation mechanisms. Basically, each mechanism consists of one or two hooks to tie down and release ERA from the mounting seats and adjustment pins to

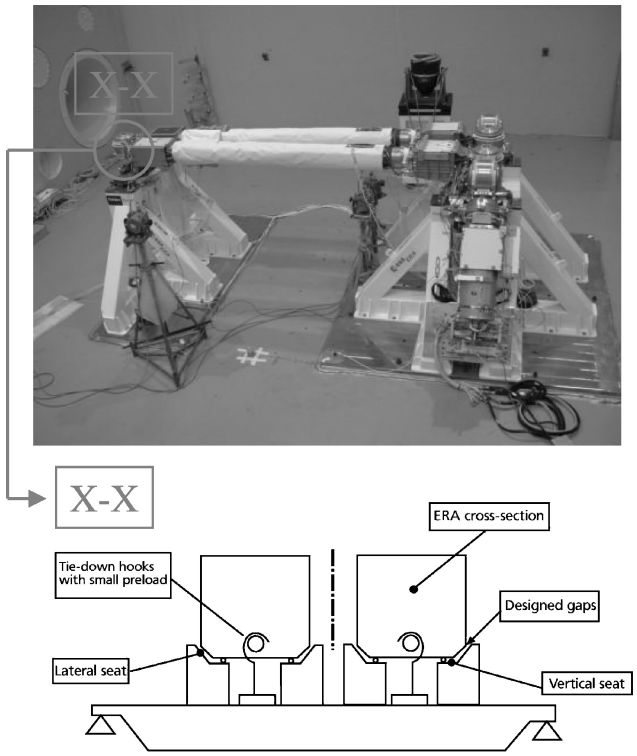

Fig. 20 Test setup and elbow attachment points of ERA.

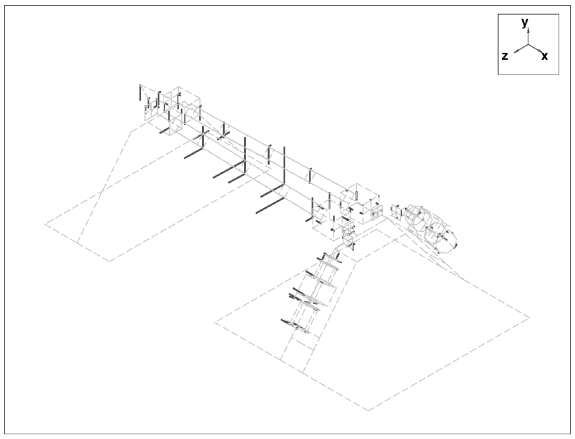

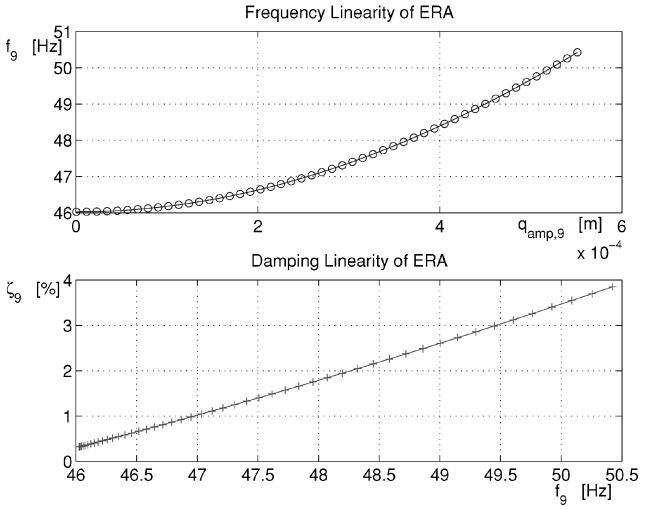

Fig. 21 Frequency and damping linearity of ERA mode 9.

control and minimize backlash. The preload in the hooks is 500 to 1000 N. Gaps between ERA and its support are introduced in order to allow for easy assembly, to cope with thermal expansion, and to ensure proper release. The test setup and a scheme for the attachment of ERA at the elbow are presented in Fig. 20. As a result of this attachment, the used modes for the qualification of the interfaces show strong, nonlinear behavior.

Here, a resonance identified at ≈46.0 Hz during the modal survey test (low forces) is used within the INTL strategy. This mode was used to qualify the interface in the vertical direction. The upper part of Fig. 21 shows the investigated mode shape. The structure was excited by a slow, narrowband, swept-sine signal around the resonance with an excitation force of 170 N. At this load level the resonance frequency was shifted to nearly 50.4 Hz. In contrast to Fig. 11, a cutout of the time-domain data from the narrowband, swept-sine run is now used for the identification process. The mode is quasi-appropriated. The generalized, linear parameters of the mode are $c_r = 70.0$ Ns/m, $m_r = 38.3$ kg, and $k_r = 3.789 \times 10^6$ N/m. The nonlinear restoring force $\delta_9(t)$ for each time step [Eq. (8)] is calculated and plotted in Fig. 22. A cubic characteristic can be observed. Next, the nonlinear restoring force without the linear stiffness term is plotted and curve fitted (Fig. 23). One-hundred-twenty-one data points are used in the identification process. Two stiffness terms are identified: a cubic stiffness $k_{\text{cub,id}} = 2.815 \times 10^{12}$ N/m^3 and a linear stiffness $k_{\text{lin,id}} = -5.856 \times 10^5$ N/m. The damping forces are plotted

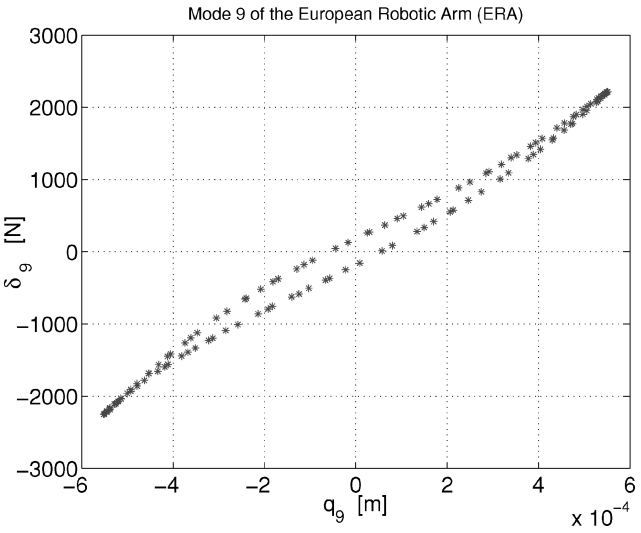

Fig. 22 Measured nonlinear restoring force including linear stiffness of ERA.

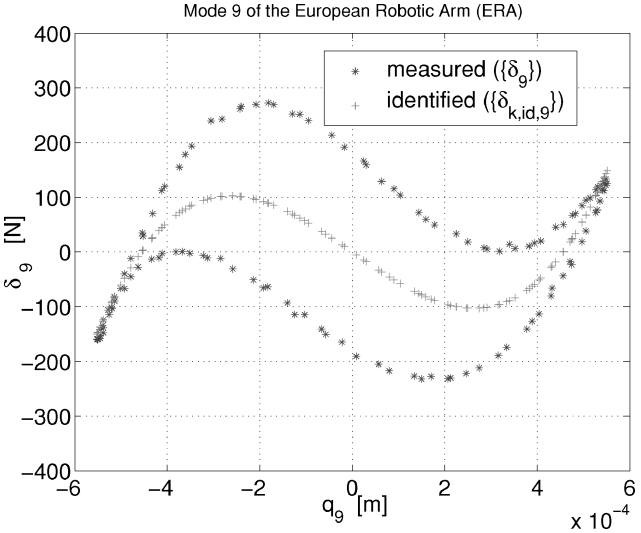

Fig. 23 Measured and identified nonlinear stiffness force of ERA.

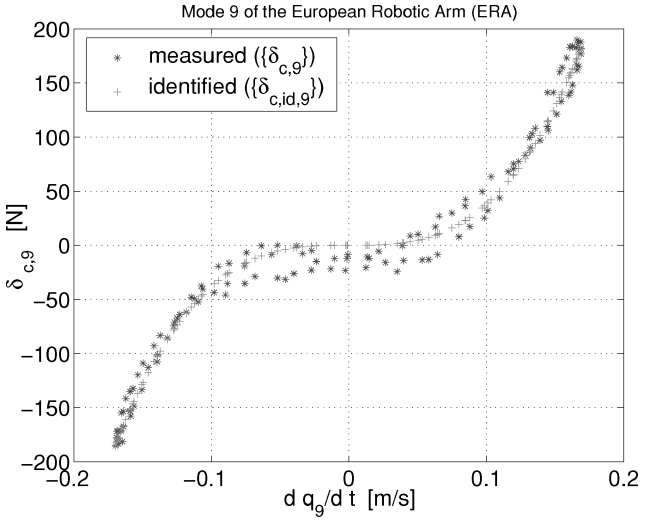

Fig. 24 Measured and identified nonlinear damping force of ERA.

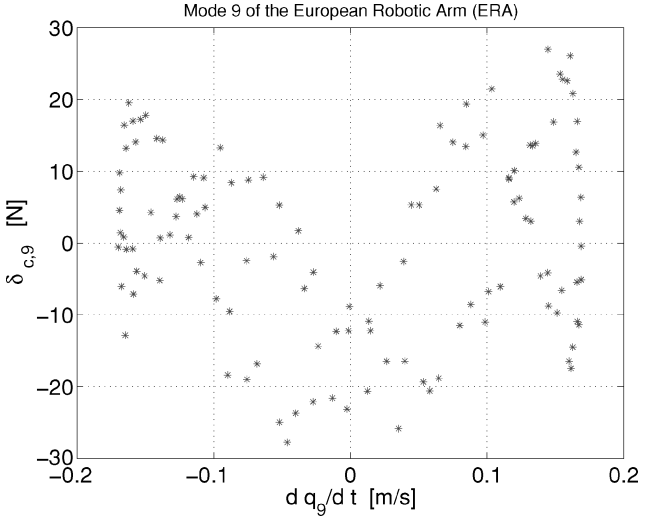

Fig. 25 Damping force after subtraction of identified nonlinear damping force of ERA.

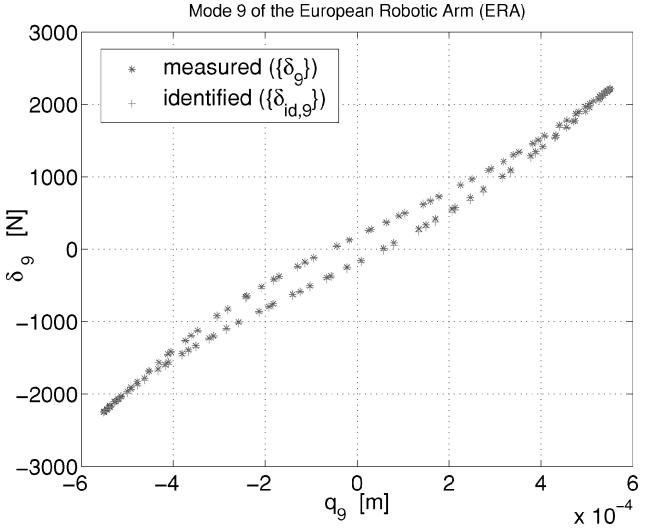

Fig. 26 Measured and identified nonlinear restoring force of ERA.

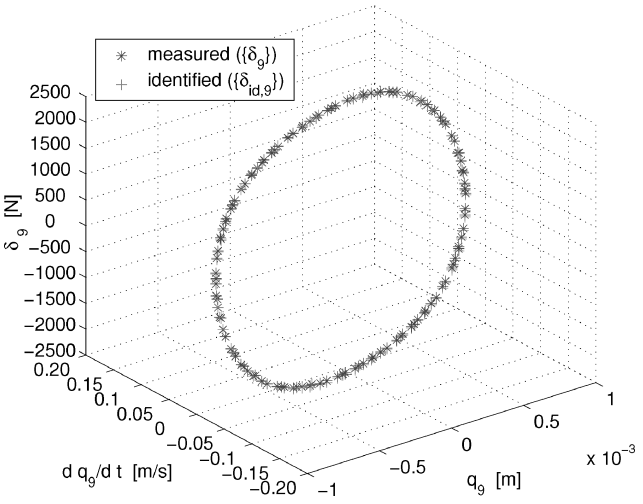

Fig. 27 Measured and identified nonlinear restoring force of ERA vs displacement and velocity.

and curve fitted in the next step. Figure 24 shows the measured and the identified damping force for the mode shape. Like in the case of stiffness identification, a cubic function is identified. The damping parameter is $c_{\text{cub,id}} = 3.779 \times 10^4$ Ns^3/m^3. To check the identified stiffnesses and damping, the residual between measured and identified damping force is plotted against the generalized velocity (see Fig. 25). The plot shows only numerical noise; the remaining force is in the scope of measurement accuracy (1.25% error). When plotting the complete measured and identified restoring force, a nearly perfect agreement can be observed (Fig. 26). Another illustration of the measured and identified restoring forces is shown in Fig. 27, where the forces are plotted vs the generalized velocity and the generalized displacements of the mode. In the last step, the dependency of the frequency and damping from the excitation level is computed for 50 points between zero and the maximum amplitude. The frequency and damping linearity plots are depicted in Fig. 21. The plots show that the resonance frequency increases by nearly 10%. The increase of the resonance frequency is caused by the increasing stiffness (see also Fig. 23). The damping also increases as a result of the increasing damping forces.

VI. Conclusions

This paper presents an advanced test strategy of modal testing that can be used to characterize and identify nonlinearities in modal space during modal survey testing. The identification approach introduced in this paper is based on the force-state mapping approach[2] and is used to identify modal, nonlinear parameters and to characterize the nonlinearity for a single mode of vibration. In a further step, a new type of linearity plot is presented, which is based on the identified restoring force of an appropriated mode shape. In contrast to common linearity plots, which are already in use during modal survey testing, this alternate method is capable of characterizing the nonlinearity from the measurement at one single excitation level. Of course, no prediction for higher excitation levels is possible. But all force levels that are lower than the measured force level can be investigated. This feature of the method helps reduce the testing time because the time-consuming tuning process for other excitation levels can be avoided. A simulated aeronautical example and a practical example taken from a boosted modal survey test on a space structure demonstrate the applicability of the presented strategy in practice.

References

[1]Göge, D., Sinapius, M., and Füllekrug, U., "Non-Linear Phenomena in Ground-Vibration Testing of Large Aircraft," *Proceedings of the International Forum on Aeroelasticity and Structural Dynamics (IFASD)*, 2003.

[2]Masri, S. F., and Caughey, T. K., "A Non-Parametric Identification Technique for Nonlinear Dynamic Problems," *Journal of Applied Mechanics*, Vol. 46, 1979, pp. 433–447.

[3]Ahlfors, L., *Complex Analysis*, 2nd ed., McGraw–Hill, New York, 1966.
[4]Simon, M., and Tomlinson, G., "Use of the Hilbert Transform in Modal Analysis of Linear and Nonlinear Structures," *Journal of Sound and Vibration*, Vol. 96, No. 4, 1984, pp. 421–436.
[5]Mertens, M., Van der Auweraer, H., Vanherck, P., and Snoeys, R., "Basic Rules of a Reliable Detection Method for Nonlinear Dynamic Behaviour," *Proceedings of the 10th International Seminar on Modal Analysis*, KU Leuven, Belgium, 1985, Pt. 4.
[6]Newland, D., *Random Vibrations, Spectral & Wavelet Analysis*, 3rd ed., Longman, 1993.
[7]Tomlinson, G., "Detection, Identification and Quantification of Nonlinearity in Modal Analysis—A Review," *Proceedings of 4th International Modal Analysis Conference (IMAC)*, 1986, pp. 837–843.
[8]Leontaritis, I., and Billings, S., "Input-Output Parametric Models for Nonlinear Systems, Part 1: Deterministic Nonlinear Systems," *International Journal of Control*, Vol. 41, No. 2, 1985, pp. 303–328.
[9]Crawley, E., and Aubert, A., "Identification of Nonlinear Structural Elements by Force-State Mapping," *AIAA Journal*, Vol. 24, No. 1, 1986, pp. 155–162.
[10]Dimitriadis, G., and Cooper, J., "A Method for Identification of Non-Linear Multi-Degree-of-Freedom Systems," *Journal of the Institute of Mechanical Engineers*, Vol. Part G 212, 1998, pp. 287–298.
[11]Rosenberg, R., "The Normal Modes of Nonlinear n-Degree-of-Freedom Systems," *Journal of Applied Mechanics*, 1962, pp. 7–14.
[12]Vakakis, A., Manevitch, L., Mikhlin, Y., Pilipchuck, V., and Zevin, A., *Normal Modes and Localisation in Non-Linear Systems*, Series in Non-Linear Science, Wiley, New York, 1996.
[13]Volterra, V., *Theory of Functions*, Blackie, 1930.
[14]Schetzen, M., *The Volterra and Wiener Theories of Non-Linear Systems*, Wiley, New York, 1980.
[15]Bendat, J., *Nonlinear System Analysis and Identification from Random Data*, Wiley, New York, 1990.
[16]Richards, C., and Singh, R., "Identification of Multi-Degree-of-Freedom Non-Linear Systems Under Random Excitation by the 'Reverse Path' Method," *Journal of Sound and Vibration*, Vol. 213, No. 4, 1998, pp. 673–708.
[17]Wright, J., Platten, M., Cooper, J., and Sarmast, M., "Identification of Multi-Degree of Freedom Weakly Non-Linear Systems Using a Model Based in Modal Space," *Proceedings of the International Conference on Structural System Identification*, COST, Kassel, 2001, pp. 49–68.
[18]Natke, H., Juang, J., and Gawronski, W., "A Brief Review on the Identification of Nonlinear Mechanical Systems," *Proceedings of 6th International Modal Analysis Conference (IMAC)*, 1988, pp. 1569–1574.
[19]Worden, K., and Tomlinson, G., *Nonlinearity in Structural Dynamics*, Inst. of Physics Publishing, 2001.
[20]Hasselmann, T., Andersson, M., and Gan, W., "Principal Components Analysis for Non-Linear Model Correlation, Updating and Uncertainty Evaluation," *Proceedings of 16th International Modal Analysis Conference (IMAC)*, 1998, pp. 644–651.
[21]Hemez, F., and Doebling, S., "Correlation and Finite Element Model Updating for Nonlinear, Transient Dynamics," *Proceedings of 17th International Modal Analysis Conference (IMAC)*, 1999, pp. 1501–1510.
[22]Gibert, C., and Thouverez, F., "Identification of the Non-Linear Modes Applied to a Structure Including a Non-Linear Component," *Proceedings of the International Conference on Structural System Identification*, COST, Kassel, 2001, pp. 183–192.
[23]Meyer, S., "Modellbildung und Identifikation von Lokalen Nichtlinearen Steifigkeits-und Dämpfungseigenschaften in Komplexen Strukturdynamischen Finite Elemente Modellen," Ph.D. Dissertation, Univ. Press Kassel, 2003.
[24]Meyer, S., and Link, M., "Local Non-Linear Softening Behaviour: Modelling Approach and Updating of Linear and Non-Linear Parameters Using Frequency Response Residuals," *Proceedings of 21st International Modal Analysis Conference (IMAC)*, 2003.
[25]Gaul, L., and Nitsche, R., "The Role of Friction in Mechanical Joints," *Applied Mechanics Reviews*, Vol. 54, No. 2, 2001.
[26]Gaul, L., and Nitsche, R., *Dynamics of Structures with Joint Connections, Structural Dynamics @ 2000*, edited by D. J. Ewins and D. J. Inman, Research Studies Press, Ltd., 2001, pp. 29–48.
[27]Link, M., and Hanke, G., *Model Quality Assessment and Model Updating*, edited by J. M. M. Silva and N. M. M. Maia, Modal Analysis and Testing, Kluwer Academic, Norwell, MA, 1999, pp. 305–324.
[28]Wright, J., Cooper, J., and Desforges, M., "Normal-Mode Force Appropriation—Theory and Application," *Mechanical Systems and Signal Processing*, Vol. 13, No. 2, 1999, pp. 217–240.
[29]Breitbach, E., "A Semi-Automatic Modal Survey Test Technique for Complex Aircraft and Spacecraft Structures," *Proceedings of 3rd ESA Testing Symposium*, 1973, pp. 519–528.
[30]Breitbach, E., "Recent Developments in Multiple Input Modal Analysis," *Journal of Vibration, Stress, and Reliability in Design*, Vol. 110, 1988, pp. 478–484.
[31]Niedbal, N., and Klusowski, E., "Die Ermittlung der Generalisierten Masse und des Globalen Dämpfungsbeiwertes im Standschwingungsversuch," *Zeitschrift für Flugwissenschaften und Weltraumforschung*, Vol. 13, No. 3, 1989, pp. 91–100.
[32]Bonneau, E., "Determination des Characteristiques Vibratoires d'une Structure a l'Aide de l'Expression de la Puissance Complex Fournie," *La Recherche Aerospatiale*, No. 130, 1969, pp. 45–51.
[33]Stearns, D., and und Hush, S. D., *Digitale Verarbeitung Analoger Signale*, R. Oldenbourg-Verlag, 1999.
[34]Worden, K., "Data Processing and Experimental Design for the Restoring Force Surface Method, Part II: Choice of Excitation Signal," *Mechanical Systems and Signal Processing*, Vol. 4, No. 4, 1990, pp. 321–344.
[35]Bogoljubov, N., and Mitropolsky, J., *Asymptotische Methoden in der Theorie der nichtlinearen Schwingungen*, Akademie Verlag, 1965.
[36]Gloth, G., and Sinapius, M., "Swept-Sine Excitation During Modal Identification of Large Aerospace Structures," DLR-Inst. für Aeroelastik, Forschungsbericht DLR-FB 2002-18, Germany, 2002.
[37]Gloth, G., and Sinapius, M., "Detection of Non-Linearities in Swept-Sine Measurements," *Proceedings of 21st International Modal Analysis Conference (IMAC)*, 2003, p. 127.
[38]Atkins, P., and Wright, J., "An Extension of Force Appropriation to the Identification of Non-Linear Multi-Degree of Freedom Systems," *Journal of Sound and Vibration*, Vol. 237, No. 1, 2000, pp. 23–43.
[39]Försching, H., *Grundlagen der Aeroelastik*, Springer-Verlag, 1974.
[40]Gloth, G., Sinapius, M., Koekenberg, A., and Berkes, U., "Boosted Modal Survey Test on the European Robotic Arm," *European Conference on Spacecraft Structures, Materials, and Mechanical Testing*, Noordwijk, The Netherlands, 2000, pp. 401–408.

A. Berman
Associate Editor